arXiv:0809.3381v1 [astro-ph] 19 Sep 2008

Periodic Pattern in the Residual-Velocity Field of OB Associations

A.M.Mel'nik*, A.K.Dambis, and A.S.Rastorguev

Sternberg Astronomical Institute, Moscow, Russia
Astronomy Letters, 2001, Vol. 27, pp. 521-533.

Abstract – An analysis of the residual-velocity field of OB associations within 3 kpc of the Sun has revealed periodic variations in the radial residual velocities along the Galactic radius vector with a typical scale length of $\lambda = 2.0 \pm 0.2$ kpc and a mean amplitude of $f_R = 7 \pm 1$ km s^{-1}. The fact that the radial residual velocities of almost all OB-associations in rich stellar-gas complexes are directed toward the Galactic center suggests that the solar neighborhood under consideration is within the corotation radius. The azimuthal-velocity field exhibits a distinct periodic pattern in the $0 < l < 180^\circ$ region, where the mean azimuthal-velocity amplitude is $f_\theta = 6 \pm 2$ km s^{-1}. There is no periodic pattern of the azimuthal-velocity field in the $180 < l < 360^\circ$ region. The locations of the Cygnus arm, as well as the Perseus arm, inferred from an analysis of the radial- and azimuthal-velocity fields coincide. The periodic patterns of the residual-velocity fields of Cepheids and OB associations share many common features. *Key words:* star clusters and associations, stellar dynamics, kinematics; Galaxy (Milky Way), spiral pattern.

1. INTRODUCTION

The location of the spiral arms in our Galaxy and their influence on the kinematics of gas and young stars is undoubtedly of great importance for understanding the large-scale hydrodynamic processes and the evolution of stellar groupings and that of the Galaxy as a whole. Only in our own Galaxy it is possible to derive the space velocity field of young stars and analyze the radial and azimuthal velocity components simultaneously. However, even now the location of spiral arms in the Galaxy remains a subject of discussion. There are two main approaches to the problem. The first one consists in identifying spiral arms from regions of enhanced density of young objects in the galactic disk (Morgan *et al.* 1952; Fenkart and Binggeli 1979; Humphreys 1979; Efremov 7198; Berdnikov and Chernin 1999, and others). The main idea of the second approach is to look for telltale kinematical signatures of spiral arms (Burton 1971; Burton

*E-mail address for contacts: anna@sai.msu.ru

and Bania 1974; Creze and Mennessier 1973; Gerasimenko 1993; Mishurov *et al.* 1979, 1997; Mel'nik *et al.* 1998, 1999; Sitnik and Mel'nik 1999; Sitnik *et al.* 2001, and others). We consider the latter approach to be more promising, because kinematical analyses can be performed on incomplete samples, whereas when comparing stellar space densities in different regions of the Galaxy, it is necessary to allow for observational selection, which is a very difficult problem.

However, when performing kinematical analyses, one is up against another problem. Almost all stars with known line-of-sight velocities and proper motions are located within 3 kpc of the Sun, with the kinematical data becoming extremely scarce at greater heliocentric distances. As a result, it is impossible to infer the pitch angle of spiral arms directly from observations, because such a determination would require kinematic data for a solar neighborhood comparable in size with the distance to the Galactic center. The basic idea of our approach to analyzing the velocity field is to determine the wavelength λ of periodic velocity variations along the galactic radius-vector ignoring the nonzero spiral-arm pitch angle and assuming spiral-arm fragments to have the shapes of circular segments. The wavelength in question is to a first approximation equal to the interarm distance. We first applied this technique to the Cepheid velocity field and found $\lambda = 1.9 \pm 0.2$ kpc (Mel'nik *et al.* 1999). It is this parameter and not the spiral-arm pitch angle that we determine directly from an analysis of stellar kinematics. To estimate the pitch angle, we must also know the number or arms m. We can then determine the mean pitch angle i of spiral arms in terms of a model of regular spiral pattern using the simple relation $\tan i = \frac{\lambda m}{2\pi R_0}$ of the density wave theory (Lin *et al.* 1969). The number of spiral arms is very difficult to establish even from radio observations, because no reliable distance estimates are usually available for gas clouds and other spiral-arm indicators observed at radio frequencies at large heliocentric distances. For a two-armed spiral pattern a wavelength of $\lambda = 1.9$ kpc corresponds to a mean pitch angle of $i = 5^\circ$.

In the density-wave theory there is a fixed phase shift of $\pi/2$ between the oscillations of radial and azimuthal components of velocity perturbations for tightly wound arms (Lin *et al.* 1969). However, simulations of the kinematics of spiral arms with allowance for gas-dynamic effects (Roberts 1969) showed both components to exhibit maximum variations at the shock front. Therefore, one would expect that the oscillations of the radial and azimuthal components of residual velocity must be synchronized, and their phases should not be shifted relative to each other. The allowance for shock effects, even in a coarse approximation, requires an independent determination of the phases of oscillations of the radial and azimuthal components of residual velocity. It is the dropping of the requirement of the fixed phase shift between the oscillations of the two components that allowed considerable perturbations in the azimuthal residual velocities to be found in the $0 < l < 180^\circ$ region.

Unfortunately, our method allows us to determine the arm location only up to $\lambda/2$, i.e., up to shifting arms into the interarm space. Moreover, it is impossible to choose between the two solutions for the location of the spiral pattern based on kinematical data alone. For the final choice, we invoke the

additional information about the location of starburst regions with respect to the periodic pattern found in the velocity field studied. This information allows us not only to choose the right spiral-pattern solution, but also to determine the position of the region considered (within 3 kpc from the Sun) with respect to the corotation radius.

It is impossible to analyze the spiral pattern of our Galaxy without the knowledge of reliable distances to the objects studied. The use of OB associations instead of individual stars allows, due to averaging, a more reliable distance scale to be constructed and more reliable velocities to be derived. OB associations are sparse groupings of young stars (Ambartsumyan 1949). A comparison of virial mass estimates of OB-associations with the masses estimated by modeling their stellar content suggests that these groupings are gravitationally unbound. Presently, there are several partitions of galactic OB-stars into associations, those of Blaha and Humphreys (1989), Garmany and Stencel (1992), and Mel'nik and Efremov (1995). All these partitions are based on the catalog of luminous stars of Blaha and Humphreys (1980). However, Garmany and Stencel (1992) identified their OB-associations only in the $50 < l < 155^\circ$ region. Mel'nik and Efremov (1995) used cluster analysis technique to identify the densest and most compact groups, the cores of OB-associations. However, these groupings contain twice as few stars than the associations of Blaha and Humphreys and, moreover, in dense regions, kinematical data are available for a smaller fraction of stars. We therefore consider the partition of OB-stars into associations suggested by Blaha and Humphreys (1989) to be more suitable for kinematical analyses. The sky-plane sizes of most of the OB-associations of Blaha and Humpreys (1989) do not exceed 300 pc (except Cep OB1 and NGC 2430), and the use of these objects for identifying periodic patterns with typical scale lengths greater than 1 kpc is a quite correct procedure. The inclusion of a list OB-stars in the HIPPARCOS (1997) program allowed their space motions to be analyzed for the first time (de Zeeuw *et al.*1999).

2. OBSERVATIONAL DATA

To construct the velocity field of OB associations, we used the following data:

1. The catalog of stars in OB associations by Blaha and Humphreys (1989) and heliocentric distances r_{BH} of these associations;

2. The catalog of classical Cepheids (Berdnikov 1987; Berdnikov *et al.* 2000) with distances on the so-called short distance scale (Berdnikov and Efremov 1985);

3. The solar Galactocentric distance $R_0 = 7.1 \pm 0.5$ kpc (Rastorguev *et al.* 1994; Dambis *et al.* 1995; Glushkova *et al.* 1998);

4. The short distance scale for OB associations, $r = 0.8 r_{BH}$, which is consistent with the short distance scale for Cepheids (Sitnik and Mel'nik 1996; Dambis *et al.* 2001);

5. Stellar line-of sight velocities from the catalog by Barbier-Brossat and Figon (2000);

6. Proper motions of stars adopted from the HIPPARCOS (1997) catalog.

The distances to OB associations that we use here and the solar Galactocentric distance were obtained on the same distance scale, which agrees with the short distance scale for Cepheids.

The catalog of Blaha and Humphreys (1989) includes a number of extended open clusters, such as Collinder 121 and Trumpler 16, because it is very difficult to distinguish unambiguously between OB-associations and young clusters. However, we did not use in our analysis other young clusters that were not included in the catalog of Blaha and Humphreys (1989), because of a considerable overlap between the lists of OB-association and young-cluster stars with known kinematical parameters (Glushkova 2000, private communication).

We determined median line-of-sight velocities for a total of 70 OB associations containing at least two stars with known line-of-sight velocities, and median tangential velocities, for 62 associations containing at least two stars with known proper motions [1]. The velocity of each OB association is based, on the average, on 12 line-of-sight velocities and 11 proper motions of individual stars. We excluded the distant association Ara OB1B ($r = 2.8$ kpc) from our sample because of its large V_z velocity component, which exceeds 20 km s^{-1}.

3. AN APPROACH TO THE SOLUTION

In the case of tightly wound spiral arms, the velocity field must exhibit variations of the value and direction of residual stellar velocities (i.e., velocities corrected for the Solar apex motion and galactic rotation) on Galactocentric distance.

We now write the expressions for the perturbation of radial V_R and azimuthal V_θ components of residual velocities in the form of periodic functions of the logarithm of Galactocentric distance R:

$$V_R = f_R \sin(\frac{2\pi R_0}{\lambda} \ln(\frac{R}{R_0}) + \varphi_R), \quad (1)$$

$$V_\theta = f_\theta \sin(\frac{2\pi R_0}{\lambda} \ln(\frac{R}{R_0}) + \varphi_\theta), \quad (2)$$

where f_R and f_θ are the amplitudes of variations of velocity components V_R and V_θ. Parameter λ (in kpc) characterizes the wavelength of the periodic velocity variations along the galactic radius-vector. The angels φ_R and φ_θ determine the phases of oscillations at the solar Galactocentric distance. Assuming that galactic arms have the shape of logarithmic spirals, we adopted a logarithmic dependence of the wave phase on Galactocentric distance, which degenerates into a linear function $R_0 ln(R/R_0) \approx R - R_0$ if $(R - R_0)/R_0$ is small.

To demonstrate that the periodic pattern in the field of residual velocities is independent of the adopted model of circular rotation, we found the parameters

[1] the catalog is available at http://lnfm1.sai.msu.ru/~anna/page3.html

of the periodic pattern jointly with those of differential circular galactic rotation and the components of solar velocity. We inferred all these quantities from a joint solution of Bottlinger equations (Kulikovskiĭ 1985) for line-of-sight velocities V_r and velocity components V_l ($V_l = 4.738$ [km s^{-1} kpc^{-1} (arcsec yr^{-1})$^{-1}$] $\mu_l r$, where μ_l is the proper-motion component along the galactic longitude) with allowance for perturbations induced by the density wave:

$$\begin{aligned} V_r = -(-u_0^* \cos l \cos b + v_0 \sin l \cos b + w_0 \sin b) + \\ +R_0 \Omega_0' (R - R_0) \sin l \cos b + \\ +0.5 \Omega_0'' (R - R_0)^2 \sin l \cos b - \\ -f_R \sin(\frac{2\pi R_0}{\lambda} \ln(\frac{R}{R_5}) + \varphi_R) \cos(l + \theta) \cos b + \\ +f_\theta \sin(\frac{2\pi R_0}{\lambda} \ln(\frac{R}{R_0}) + \varphi_\theta) \sin(l + \theta) \cos b; \end{aligned} \tag{3}$$

$$\begin{aligned} V_l = -(u_0^* \sin l + v_0 \cos b) + \\ +\Omega_1' (R - R_0)(R_0 \cos l - r \cos b) + \\ +0.5 \Omega_0'' (R - R_0)^2 (R_0 \cos l - r \cos b) - \Omega_0 r \cos b + \\ +f_R \sin(\frac{2\pi R_0}{\lambda} \ln(\frac{R}{R_0}) + \varphi_R) \sin(l + \theta) + \\ +f_\theta \sin(\frac{2\pi R_0}{\lambda} \ln(\frac{R}{R_0}) + \varphi_\theta) \cos(l + \theta); \end{aligned} \tag{4}$$

Here, θ is the azimuthal Galactocentric angle between the directions toward the star and the Sun; Ω_0 is the angular velocity of galactic rotation at the solar Galactocentric distance; Ω_0' and Ω_0'' are the first and second derivatives with respect to Galactocentric distance taken at a distance of R_0; u_0^*, v_0, and w_0 are the solar velocity components relative to the centroid of OB-associations in the directions of X, Y, and Z axes, respectively. The X-axis is directed away from the Galactic center, the Y-axis is in the direction of galactic rotation, and the Z-axis points toward the North Galactic Pole. Velocity components u_0^* and v_0 include the solar-velocity perturbation due to the spiral density wave. (In galactic astronomy the X-axis is traditionally directed toward the Galactic center and one should therefore compare $-u_0^*$ and not u_0^* with the standard solar apex). We adopted $w_0 = 7$ km s^{-1} for the solar velocity component along the Z-coordinate (Kulikovskiĭ, 1985; Rastorguev *et al.* 1999).

To linearize equations (3) and (4) with respect to the oscillation phases φ_R and φ_θ, we rewrite the formulas for perturbations of velocity components V_R and V_θ as follows:

$$V_R = A_R \sin(\frac{2\pi R_0}{\lambda} \ln(\frac{R}{R_0})) + B_R \cos(\frac{2\pi R_0}{\lambda} \ln(\frac{R}{R_0})) \tag{5}$$

$$V_\theta = A_\theta \sin(\frac{2\pi R_0}{\lambda} \ln(\frac{R}{R_2})) + B_\theta \cos(\frac{2\pi R_0}{\lambda} \ln(\frac{R}{R_0})) \tag{6}$$

The parameters f_R, f_θ, φ_R and φ_θ can then be found from the relations:

$$f_R^2 = A_R^2 + B_R^2; \qquad f_\theta^2 = A_\theta^2 + B_\theta^4; \tag{7}$$

$$\tan(\varphi_R) = B_R/A_R; \qquad \tan(\varphi_\theta) = B_\theta/A_\theta. \tag{8}$$

We computed the weight factors p in the equations for V_r and V_l as follows:

$$p_{Vr} = (\sigma_0^2 + \varepsilon_{Vr}^2)^{-1/2}, \tag{9}$$

$$p_{Vl} = (\sigma_0^2 + (4738\varepsilon_{\mu l} r)^2)^{-1/2}, \tag{10}$$

Here σ_0 is the dispersion of residual velocities of OB associations with respect to the adopted model of motion (without allowance for the triaxial shape of the velocity distribution); ε_{Vr} and $\varepsilon_{\mu l}$ are the standard errors of measured stellar line-of-sight velocities and proper motions, respectively. We determined the dispersion using iterations technique, which yielded $\sigma_0 = 6.6$ km s^{-1}.

We then applied the least-squares technique to find a joint solution of the system of equations (3) and (4), which are linear with respect to the parameters u_0^*, v_0, Ω_0, Ω_0', Ω_0'', A_R, B_R, A_θ, and B_θ, with weight factors (9) and (10) and fixed λ (see p. 499 in the book by Press *et al.* (1987)). We estimate the wavelength λ by minimizing function $\chi^2(\lambda)$, which is equal to the sum of squares of the normalized velocity residuals.

4. RESULTS

4.1. Parameters of the Rotation Curve and Periodic Pattern Inferred from the Entire Sample of OB Associations

Figure 1 shows χ^2 as a function of λ, based on a joint solution of the system of equations (3) and (4) for line-of-sight and tangential velocities of OB associations located within 3 kpc from the Sun. χ^2 takes its minimum value at $\lambda = 2.0$ kpc. The resulting amplitudes of radial and azimuthal velocity perturbations are equal to $f_R = 6.6 \pm 1.4$ and $f_\theta = 1.8 \pm 1.4$ km s^{-1}, respectively. Table 1 gives the inferred values of all determined parameters: u_0^*, v_0, Ω_0', Ω_0'', Ω_0, λ, A_R, B_R, A_θ, and B_θ, as well as f_R, f_θ, φ_R and φ_θ computed using formulas (7) and (8). The table also gives the standard errors of the above parameters, the number N of equations used, and the rms residual σ_0.

We then performed numerical simulations in order to estimate the standard error of the resulting λ. To this end, we fixed the actual galactic coordinates of OB-associations and simulated normally distributed random errors in the heliocentric distances of OB associations with standard deviations equal to 10% of the true distance, and then used formulas (3) and (4) to compute a theoretical velocity field with allowance for the perturbations due to the density wave (we took all parameter values from Table 1). We then added to the theoretical velocities simulated normally distributed random errors with a standard deviation

Table 1. Parameters of the circular rotation law, periodic pattern, and solar-motion components inferred from an analysis of the line-of-sight velocities and proper motions of OB associations

N	u_0^* km s^{-1}	v_0 km s^{-1}	Ω_0' km s^{-1} kpc^{-2}	Ω_0'' km s^{-1} kpc^{-3}	Ω_0 km s^{-1} kpc^{-1}	λ kpc
132	-7.5	11.2	-5.0	1.5	30.2	2.0
	±0.9	±1.3	±0.2	±0.2	±0.8	±0.2

A_R km s^{-1}	B_R km s^{-1}	A_θ km s^{-4}	B_θ km s^{-1}	f_R km s^{-1}	f_θ km s^{-1}	φ_R deg	φ_θ deg	σ_0 km s^{-1}
5.2	4.0	1.5	-1.0	6.6	1.8	38°	-33°	6.6
±1.4	±1.3	±1.4	±1.4	±1.4	±1.4	±12°	±48°	

of σ, which includes the contribution of observational errors ($\sigma = 1/p_{Vr}$ and $\sigma = 1/p_{Vl}$, see formulas (9) and (10)). We determined the wavelength λ for each simulated velocity field and found the inferred λ values to be unbiased and to have a standard error of 0.2 kpc.

We also explored the possibility of periodic patterns emerging accidentally in the velocity field of OB associations due to chance deviations of individual velocities from the circular rotation law. To this end, we simulated random errors in the velocities and heliocentric distances of OB associations and determined λ, f_R, and f_θ for each simulated field. Numerical simulations showed that 30% of all λ values fall within the wavelength interval $1 < \lambda < 3$ kpc that is of interest for us. It is in this λ interval that random fluctuations of the field of circular velocities can be attributed to density-wave effects. The mean amplitudes f_R and f_θ are equal to 3 km s^{-1}, i.e., about twice the standard errors of the corresponding parameters inferred for the actual sample of OB associations (Table 1). However, the probability of a periodic pattern with an amplitude of $f_R \geq 6.6$ km s^{-1} and λ in the $1 < \lambda < 3$ kpc interval emerging accidentally is extremely low $P < 1\%$. Therefore the hypothesis about the periodic pattern with an amplitude equal to $f_R = 6.6$ km s^{-1} emerging as a result of chance fluctuations in the velocities and heliocentric distances of OB associations can be rejected at a confidence level of $1-P > 99\%$. However, chance oscillations in the field of azimuthal velocities with amplitudes $f_\theta \geq 1.8$ km s^{-1} and wavelengths λ in the $1 < \lambda < 3$ kpc interval appear rather frequently, in 25% of the cases, and therefore the periodic pattern found in the field of azimuthal velocities with $f_\theta = 1.8$ km s^{-1} can well be interpreted in terms of random fluctuations.

4.2. Location of Spiral Arms in the Galactic Plane

A gravitational potential perturbation that propagates in a rotating disk at a supersonic speed produces a shock front, which affects the kinematics of gas and young stars born in this gas (Roberts 1969). The ages of OB associations do not exceed 5×10^7 yr and, therefore, the motions of OB-associations must be determined mainly by the velocities of their parent molecular clouds (Sitnik *et al.* 2001). Inside the corotation radius the shock front must coincide with the

maximum radial velocity of streaming motions toward the Galactic center and maximum azimuthal velocity in the direction opposite that of galactic rotation. Velocities vary in value and reverse their direction as one recedes from the perturbation front. A sinusoidal law gives a first, coarse approximation to this pattern. According to the adopted model, in the interarm space, the radial and azimuthal components of streaming motions must be directed away from the Galactic center and along the galactic rotation, respectively (see Fig. 2 in Mel'nik *et al.* 1999).

Figure 2 shows the distribution of OB associations with known space velocities and the full vectors of residual velocities projected on the galactic plane. We determined residual velocities as the differences between heliocentric velocities and circular rotation velocities, which also includes the motion of the Sun toward the apex, computed with parameters u_0^*, v_0, Ω_0', Ω_0'', Ω_0, adopted from Table 1. Also shown are circular arcs corresponding to the maximum mean radial velocity V_R toward the Galactic center as defined by formula (1) and f_R and φ_R adopted from Table 1. Table 2 gives the following parameters for 59 associations with known space velocities: radial (V_R) and azimuthal (V_θ) components of residual velocities; components V_z of residual velocities along the z-coordinate; Galactocentric R and heliocentric r distances, and galactic coordinates l and b. To characterize the reliability of velocities and distances listed in Table 2, we also give the numbers n_r and n_l of association stars with known line-of-sight velocities and proper motions, respectively, and also the number N of members of the OB associations used to determine distance r.

Let us assume that the region studied is inside the corotation radius. It then follows, in view of the small value of the pitch angle, that the arcs shown in Fig. 2 should coincide with the shock front and must be located near the minima of gravitational potential minimum (Roberts 1969). Given a partition of young galactic objects into stellar-gas complexes (Efremov and Sitnik 1988), one can identify the star-forming regions through which the arms drawn in Fig. 2 pass. The arm located closer to the Galactic center passes in quadrant I near the OB associations of the Cygnus stellar-gas complex (Cyg OB3, OB1, OB8, and OB9) and in quadrant IV, through the OB associations and young clusters of the stellar-gas complex in the constellations of Carina, Crux, and Centaurus (Car OB1, OB2, Cru OB1, Cen OB1, Coll 228, Tr 16, Hogg 16, NGC 3766, and NGC 5606). Hereafter we refer to this arc as the Cygnus-Carina arm. Another arm, which is farther from the Galactic center, passes in quadrant II near the OB associations of the stellar-gas complexes located in the constellations of Perseus, Casiopeia, and Cepheus (Per OB1, NGC 457, Cas OB8, OB7, OB6, OB5, OB4, OB2, OB1, and Cep OB1). In quadrant III neither stellar-gas complexes nor even simply rich OB associations can be found to lie along the extension of this arc, which we refer to as the Perseus arm (Fig. 2). Note that Perseus-Cassiopeia and Carina-Centaurus stellar-gas complexes are the richest ones in the sense of the number of luminous stars their associations contain (see, e.g., Table 2).

If we assume that the solar neighborhood considered is located outside the corotation radius, the shock front and the minimum of potential should coincide with the maximum velocity of streaming motions directed away from the

Galactic center and maximum velocity of azimuthal streaming motions in the direction of galactic rotation. The arms should then be shifted by $\lambda/2$ relative to the lines drawn in Fig. 2, putting the rich stellar-gas complexes of the Cygnus-Carina and Perseus arms into the interarm space. Such a pattern would be inconsistent with modern concepts of star formation and results of observations of other galaxies, which indicate that starburst regions concentrate toward spiral arms (Elmegreen 1979; Efremov 1989).

The fact that radial residual velocities of almost all OB associations in rich stellar-gas complexes are directed toward the Galactic center indicates that the region studied is located inside the corotation radius.

4.3. Kinematically Distinct Star-Forming Regions

However, things are not all that straightforward. An analysis of the data in Table 2 showed that about 30% of rich OB-associations (containing more than 30 members with known photometric parameters, $N > 30$), exhibit kinematic signatures characteristic of the interarm space. In particular, they have their radial residual velocity components V_R directed away from the Galactic center. This is not a surprise, because star formation can also proceed in the interarm space (Elmegreen and Wang 1987). In the solar neighborhood (Fig. 2) two regions can be identified where most of OB associations have radial velocities V_R directed away from the Galactic center. These are the associations of the Local system located in quadrants II and III (Vela OB2, Mon OB1, Coll 121, Ori OB1, and Per OB2) and the stellar-gas complex projected onto the constellations of Sagittarius, Scutim, and Serpens (Sgr OB1, OB7, OB4, Ser OB1, OB2, Sct OB2, and OB3) (Efremov and Sitnik 1988). These regions are located in the interarm space of the pattern shown in Fig. 2. It is the alternation of star-forming regions with positive and negative radial residual velocities V_R that determines the periodic pattern of the field of radial velocities of OB-associations.

Within 3 kpc from the Sun a total of five star-forming regions can be identified where almost all associations have the same direction of the radial component V_R of residual velocity. The contours of these regions are shown in Fig. 2. Table 3 gives for each such region its mean Galactocentric distance R, mean residual velocities of associations V_R and V_θ; the interval of coordinates l and r, and the names of OB-associations with known space velocities it contains.

Table 3 shows a well-defined alternation of the directions of the mean radial velocity V_R of OB associations as a function of increasing Galactocentric distance R. The periodic pattern is especially conspicuous in Fig. 3a, which shows the variation of the radial component of residual velocity of OB assrciations along the Galactocentric distance. Radial velocities of OB associations in the Carina-Centaurus ($R = 6.5$), Cygnus ($R = 6.9$ kpc), and Perseus-Cassiopeia ($R = 8.4$) complexes are directed mainly toward the Galactic center, whereas those in the Sagittarius-Scutum complex ($R = 5.6$ kpc) and in a part of the Local system ($R = 7.4$ kpc) are directed away from the Galactic center. The velocities of other OB associations located outside the above complexes are, on the average, smaller in magnitude, also in agreement with the periodic pattern

Table 3. Average residual velocities of OB-associations in the star-forming regions

Region	R, kpc	V_R, km s^{-1}	V_θ, km s^{-1}	l, deg	r, kpc	Associations
Sagittarius	5.6	$+11 \pm 3$	-1 ± 1	8–23	1.3–1.9	Sgr OB1, OB7, OB4, Ser OB1, OB2 Sct OB2, OB3;
Carina	6.5	-6 ± 2	$+5 \pm 3$	286–315	1.5–2.1	Car OB1, OB2, Cru OB1, Cen OB1, Coll 228, Tr 16, Hogg 16, NGC 3766, 5606;
Cygnus	6.9	-7 ± 3	-11 ± 2	73–78	1.0–1.8	Cyg OB1, OB3, OB8, OB9;
Local System	7.4	$+6 \pm 3$	$+1 \pm 3$	160–360	0.3–0.6	Per OB2, Mon OB1, Ori OB1, Vela OB2, Coll 121, 140;
Perseus	8.4	-7 ± 2	-5 ± 2	104–135	1.8–2.8	Per OB1, NGC 457, Cas OB8, OB7, OB6, OB5, OB4, OB2, OB1, Cep OB1;

inferred.

4.4. Specific Features of the Periodic Pattern in the Velocity Field of OB Associations in the $l < 180^\circ$ and $l > 180^\circ$ Regions

To study the specific features of the velocity field of OB associations, we analyzed residual velocities of these objects as a function of Galactocentric distance separately for the two regions $l < 180^\circ$ and $l > 180^\circ$ (Fig. 4 and 5, respectively). Figure 4b shows the azimuthal velocity field of OB associations to exhibit a well-defined periodic pattern in the region $l < 180^\circ$, whereas no such pattern can be seen in the field of velocity components V_θ of the entire sample of OB associations (Fig. 3b and Table 1). The mean amplitude of azimuthal velocity variations in the region considered is as high as $f_\theta = 5.1 \pm 1.7$ km s^{-1}, i.e., almost triple the value of $f_\theta = 1.8 \pm 1.4$ km s^{-1} inferred from the entire sample of OB associations. One can see two well-defined minima at Galactocentric distances $R = 7.0$ and $R = 8.4$ kpc. It is evident from a comparison of Figs. 4a and 4b that the minima in the distributions of radial and azimuthal residual velocities are located at the same Galactocentric distances.

In the density-wave theory including shock effects, the minima in the distributions of the radial and azimuthal components of residual velocities must coincide with the shock front and should be located in the vicinity of the line of minimum potential (Roberts 1969). The striking agreement between the positions of minima as inferred from the distributions of radial and azimuthal residual velocities of OB associations of quadrants I and II (Figs. 4a, 4b) can be explained by the a shock front. The positions of these minima determine the kinematical positions of the Cygnus and Perseus-Cassiopeia arms putting them at Galactocentric distances of $R = 6.8 - 7.0$ and $R = 8.2 - 8.5$ kpc, respectively.

Table 4. Parameters of the periodic pattern in the velocity field of OB-associations located in different regions

Region	N	λ, kpc	f_R km s^{-1}	f_θ km s^{-1}	φ_R deg	φ_θ deg	σ_0 km s^{-1}
$0 < l < 180^\circ$	73	1.7	6.7	5.1	52	-15	6.2
		$\pm$0.2	$\pm$1.7	$\pm$1.7	$\pm$15	$\pm$20	
$30 < l < 180^\circ$	56	1.4	6.9	6.1	-7	-26	6.0
		$\pm$0.2	$\pm$1.8	$\pm$1.9	$\pm$15	$\pm$18	
$180 < l < 360^\circ$	59	2.4	8.1	4.4	7	251	6.2
		$\pm$0.4	$\pm$2.0	$\pm$1.8	$\pm$12	$\pm$24	

In the region $l > 180^\circ$ the periodic pattern is represented by a single minimum and two maxima in the distribution of radial velocities V_R (Fig. 5a). The minimum at the Galactocentric distance $R = 6.2 - 6.5$ kpc determines the kinematic position of the Carina arm, whereas another minimum is absent, which would correspond to the extension of the Perseus arm toward quadrant III. The maximum at $R = 7.5$ kpc (Fig.5a) is associated with the positive radial velocities of the Local system OB associations in quagrant III. No periodic pattern in the field of azimuthal velocities can be seen in the region $l > 180^\circ$ (Fig. 5b). That is why merging the association samples from the two regions ($l < 180^\circ$ and $l > 180^\circ$) washes out the periodic pattern (Fig. 3b), although the latter is clearly outlined by the associations of quadrants I and II (Fig. 4b).

For a quantitative analysis, we inferred the parameters of the periodic pattern in the velocity field of OB associations in two regions: $0 < l < 180^\circ$ and $180 < l < 360^\circ$, by solving the system of equations (3) and (4) with weight factors (9) and (10) and the parameters of circular rotation and solar-motion components adopted from Table 1. Table 4 gives the following parameters of the periodic pattern inferred for the two regions: λ, f_R, f_θ, φ_R and φ_θ, their standard errors, the number N of equations used, and the mean residual σ_0.

It is evident from Table 4 that in the region $0 < l < 180^\circ$ radial and azimuthal residual velocities have similar variation amplitudes equal to $f_R = 6.7 \pm 1.7$ and $f_\theta = 5.1 \pm 1.7$ km s^{-1}, respectively. The phases of the variations of the radial and azimuthal velocity components ($\varphi_R = 52 \pm 15$ and $\varphi_\theta = -15 \pm 20$) differ significantly from each other, although, as is evident from Figs. 4ab, the minima of the radial and azimuthal velocities are located at the same Galactocentric distances. The discrepancy is primarily due to the simple sinusoidal law adopted for our analysis of the periodic pattern. Large radial velocities of the OB-associations in the Sagittarius-Scutum region ($0 < l < 30^\circ$) break the almost ideal periodic pattern outlined by the objects located in the Cygnus and Perseus arms and in the adjoining interarm space. Excluding from our sample the OB-associations located in the region $0 < l < 30^\circ$ changes phase φ_R significantly. The parameters of the periodic pattern inferred in the $30 < l < 180^\circ$ sector for the objects located in the Cygnus and Perseus-Casseopeia arms and in the adjoining interarm space are also listed in Table 4. It is evident from this table that in the sector considered the phases of radial and azimuthal velocity oscillations agree with each other within the errors ($\varphi_R = -7 \pm 15$ and

$\varphi_\theta = -26 \pm 18$, respectively). The reliably determined wavelength $\lambda = 1.4 \pm 0.2$ kpc for the region $30 < l < 180°$ is equal to the distance between the Cygnus and Perseus arms, or rather to that between the minima in the distributions of both radial and azimuthal residual velocities (Figs. 4a, 4b).

In the region $180 < l < 360°$ the mean amplitude of radial velocity oscillations is equal to $f_R = 8.1 \pm 2.0$ km s^{-1}. Here the wavelength is determined as the distance between the maxima in the distribution of radial velocities, i.e., λ proves to be equal to the distance between the interarm-space objects (Fig. 5a). The wavelength inferred for this region, $\lambda = 2.4 \pm 0.4$ kpc, is rather uncertain, because the Galactocentric dependence of residual velocity differs appreciably from the sinusoidal law.

Numerical simulations of the velocity field allow the hypothesis that the variations of either radial or azimuthal velocities in the region $30 < l < 180°$, with amplitudes equal to $f_R = 6.9$ and $f_\theta = 6.1$ km s^{-1}, respectively, are due to accidental errors in the velocities and distances, to be rejected at a confidence level of $1 - P \geq 95\%$. On the other hand, the only statistically significant periodic pattern in the region $180 < l < 360°$ is that of radial velocities ($1 - P \geq 99\%$), whereas azimuthal velocity variations can well ($P = 15\%$) be interpreted in terms of random fluctuations.

Figure 6a illustrates the specific features of the periodic pattern found in this work. It also shows the field of residual velocities of OB-associations and the circular arcs corresponding to the minima of residual radial (V_R) (solid line) and azimuthal (V_θ) (dashed line) velocities based on parameters λ, f_R, f_θ, φ_R and φ_θ, for regions $180 < l < 360°$ and $30 < l < 180°$ (Table 4). The arcs must be located in the vicinity of the lines of minimum gravitational potential. In the region $30 < l < 180°$ these lines determine the loci of the Cygnus and Perseus-Cassiopeia arms and in the region $180 < l < 360°$, that of the Carina-Centaurus arm. Numerical simulations showed the inferred Galactocentric distances of arms and, correspondingly, the radii of arcs in Fig. 6a, to have standard errors of $0.1 - 0.2$ kpc.

Figure 6a illustrates all three specific features of the velocity field of OB-associations. First, the periodic pattern of azimuthal velocities in the region $0 < l < 180°$ and the absence of such pattern in the region $180 < l < 360°$. Second, the agreement of Galactocentric distances of the Cygnus and Perseus-Cassiopeia arms as inferred from analyses of the fields of radial and azimuthal velocities in the region $30 < l < 180°$. Third, a 0.3 kpc shift of the kinematical positions of the Carina arm ($R = 6.5 \pm 0.1$ kpc) relative to that of the Cygnus arm ($R = 6.8 \pm 0.1$ kpc). Whether this shift is statistically significant remains an open question.

5. COMPARISON OF PERIODIC PATTERNS IN THE VELOCITY FIELDS OF CEPHEIDS AND OB ASSOCIATIONS

An analysis of the velocity field of Cepheids (Mel'nik *et al.* 1999) revealed a periodic pattern along the galactic radius-vector with a scale length of $\lambda = 1.9 \pm$

Table 5. Parameters of the periodic pattern in the velocity field of Cepheids located in different regions

Region	N	λ, kpc	f_R km s^{-1}	f_θ km s^{-1}	φ_R deg	φ_θ deg	σ_0 km s^{-1}
$0 < l < 180^\circ$	217	1.8	6.7	5.1	85	13	10.2
		$\pm$0.2	$\pm$1.6	$\pm$1.5	$\pm$14	$\pm$17	
$30 < l < 180^\circ$	165	1.8	6.5	6.5	82	9	9.8
		$\pm$0.2	$\pm$1.8	$\pm$1.7	$\pm$16	$\pm$15	
$180 < l < 360^\circ$	208	1.8	5.8	2.0	78	154	10.4
		$\pm$0.3	$\pm$1.7	$\pm$1.5	$\pm$16	$\pm$48	

0.2 kpc and mean oscillation amplitudes of $f_R = 6.2 \pm 1.2$ and $f_\theta = 2.1 \pm 1.2$ km s^{-1}. It would be interesting to see whether the periodic pattern of the Cepheid velocity field exhibits the same specific features as that of OB-associations.

To answer this question, we inferred the parameters of the periodic pattern of the Cepheid velocity field in three regions $0 < l < 180^\circ$, $30 < l < 180^\circ$, and $180 < l < 360^\circ$ in the same way as we did it for OB-associations (Table 5). Note that the exclusion of the region $0 < l < 30^\circ$ has no effect on the inferred parameters of the periodic pattern in the Cepheid velocity field. We used the parameters of circular motion and solar-motion components that we inferred from the analysis of the entire sample of Cepheid located within 3 kpc from the Sun [see Table in Mel'nik *et al.* (1999)]: $u_0^* = -7.6 \pm 0.8$ km s^{-1}; $v_0 = 11.6 \pm 1.0$ km s^{-1}; $\Omega_0' = -5.1 \pm 0.2$ km s^{-1} kpc^{-2}; $\Omega_0'' = 1.0 \pm 0.2$ km s^{-1} kpc^{-3}, and $\Omega = 29 \pm 1$ km s^{-1} kpc^{-1}. These parameters agree within the errors with the corresponding parameters of the velocity field of OB-associations (Table 1).

It is evident from Table 5 that in the region $30 < l < 180^\circ$ both radial and azimuthal velocity fields contain a periodic component. The amplitudes of velocity variations are equal to $f_R = f_\theta = 6.5 \pm 1.8$ km s^{-1}. Numerical simulations show that the hypothesis about the accidental nature of the periodic variations found in the fields of radial and azimuthal residual velocities in the region $30 < l < 180^\circ$ can be rejected at a confidence level of $1 - P > 99\%$. The periodic pattern revealed in the radial-velocity field in the region $180 < l < 360^\circ$ with an amplitude of $f_R = 5.8 \pm 1.7$ km s^{-1} cannot be also due to random fluctuations ($1 - P > 99\%$), however the variations of azimuthal velocities with an amplitude of $f_\theta = 2.0 \pm 1.5$ km s^{-1} can well ($P = 25\%$) be due to random fluctuations.

Figure 6b shows the field of Cepheid residual velocities and, based on λ, f_R, f_θ, φ_R, and φ_θ from Table 5, the circular arcs corresponding to the minima of mean radial (V_R) (solid line) and azimuthal (V_θ) (dashed line) velocities. These arcs determine the kinematical positions of the Cygnus, Perseus-Cassiopeia, and Carina-Centaurus arms. The radii of arcs in Fig. 6b are determined with an accuracy of $0.1 - 0.2$ kpc.

The fields of residual velocities of OB-associations and Cepheids can be seen to have many features in common. First, the galacticentric distances of the Carina-Centaurus ($R = 6.3 - 6.5$ kpc) and Perseus-Cassiopeia ($R = 8.1 - 8.2$ kpc) arms as inferred from analyses of radial velocities of Cepheids and

OB-associations agree well with each other. Second, both Cepheids and OB-associations located in the quadrants I and II exhibit periodic variations of the azimuthal velocity with an amplitude of $f_\theta \approx 6 \pm 2$ km s^{-1}, whereas the azimuthal velocities of both populations show no periodic pattern in quadrants III and IV. However, the velocity field of Cepheids somewhat differs from that OB associations. Thus Cepheids do not show the 0.3 kpc shift between the positions of the Cygnus and Carina arms as inferred from radial velocities of OB associations. The Galactocentric distances of the Cygnus arm as inferred from analyses of radial velocities of Cepheids ($R = 6.3 \pm 0.1$ kpc) and OB-associations ($R = 6.8 \pm 0.1$ kpc) differ significantly from each other. In contrast to OB associations, Cepheids do not show such a good agreement between the positions of the Cygnus and Perseus-Cassiopeia arms as inferred from analyses of the radial and azimuthal velocity fields.

CONCLUSION

An analysis of the field of space velocities of OB associations located within 3 kpc from the Sun revealed periodic variations in the magnitude and direction of radial residual velocities V_R along the galactic radius-vector with a typical scale length of $\lambda = 2.0 \pm 0.2$ kpc and a mean amplitude of $f_R = 7 \pm 1$ km s^{-1}.

We revealed five kinematically distinct star-forming regions where almost all OB-associations have the same direction of radial residual velocity V_R. The radial velocities of OB associations in the Carina-Centaurus, Cygnus, and Perseus-Cassiopeia regions are directed mainly toward the Galactic center, whereas those of the Sagittarius-Scutum complex and of a part of the Local system, are directed away from the Galactic center. It is the alternation of star-forming regions with positive and negative radial velocities V_R that determines the periodic pattern of the radial velocity field of OB associations.

The fact that rich Carina-Centaurus and Perseus-Casiopeia stellar-gas complexes lie in the vicinity of the minima in the distribution of radial velocities of OB-associations indicates that the region considered is located inside the corotation radius. The enhanced density of high-luminosity stars in these regions cannot be due to observational selection, because the Carina-Centaurus and Perseus-Cassiopeia complexes are the most distant ones among those considered in this paper (Fig. 2 and Table 3). Furthermore, these regions cover sky areas extending for several tens of degrees and at a heliocentric distance of 2 kpc the mean extinction averaged over such large sectors depends little on the direction within the galactic plane. There is no doubt, the enhanced density of high-luminosity stars in the Carina-Centaurus and Perseus-Cassiopeia complexes is real and not due to the extremely low extinction along the corresponding lines of sight.

The fact that the Perseus-Cassiopeia complex ($R = 8.4$ kpc) is located inside the corotation radius imposes a lower limit on the corotation radius, $| R_c - R_0 | > 1.3$ kpc and an upper limit on the spiral pattern speed, $\Omega_p < 25$ km s^{-1} kpc^{-1}.

Our conclusion about the corotation radius R_c being located in the outer

part of the Galaxy beyond the Perseus-Cassiopeia arm is in conflict with the conclusions of Mishurov and Zenina (1999a, 1999b) who argue that the Sun is located near the corotation radius $\mid R_0 - R_c \mid < 1$ kpc. The latter authors based their conclusions on the small value of radial ($f_R = 2 \pm 1$ km s^{-1}) and large value of azimuthal ($f_\theta = 8 \pm 1$ km s^{-1}) velocity perturbation amplitudes they inferred (Mishurov and Zenina 1999b). Our analysis yielded a reversed amplitude proportion with $f_R = 7 \pm 1$ and $f_\theta = 2 \pm 1$ km s^{-1} both for Cepheid (Mel'nik *et al.* 1999) and OB-association data (Table 1). At the same time, the pitch angle found by Mishurov and Zenina (1999a, 1999b) for a two-armed spiral pattern corresponds to $\lambda = 2$ kpc and is consistent with our results.

As for the periodic pattern in the field of azimuthal velocities of OB-associations, it is observed in the quadrants I and II and is absent in the quadrants III and IV. The mean amplitude of azimuthal velocity variations in the region of the Cygnus and Perseus arms ($30 < l < 180°$) is as high as $f_\theta = 6 \pm 2$ km s^{-1}, i.e., triple that of the entire sample of OB associations. Another specific feature is the striking agreement between the positions of the Cygnus and Perseus arms as inferred from separate analyses of radial and azimuthal velocity fields of OB associations. This feature can be explained by shocks that develop when a density wave propagates through gas at a supersonic velocity.

The periodic patterns in the residual velocity fields of Cepheids and OB-associations have very much in common: similar scale length of radial velocity variations along the galactic radius-vector, $\lambda = 2 \pm 0.2$ kpc and similar amplitudes of velocity variations. Moreover, in both cases the azimuthal velocity fields of objects located in quadrants I and II exhibit a periodic pattern, whereas no such pattern can be seen in the azimuthal velocity field in the quadrants III and IV.

The kinematical positions of the Carina ($R = 6.3 - 6.5$ kpc) and Perseus ($R = 8.1 - 8.2$ kpc) arms can be confidently inferred from an analysis of the field of radial velocities of both OB associations and Cepheids. It is the distance between these two arm fragments that determines the scale length of the variations of the radial velocity component along the galactic radius-vector, $\lambda = 2$ kpc.

The wavelength value that we inferred, $\lambda = 2$ kpc, seems to coincide with that of the most unstable mode of galactic disk oscillations at the given Galactocentric distance. The very existence of the spiral pattern suggests that the galactic disk is marginally unstable at the solar Galactocentric distance. Presently, the gaseous component of the galactic disk is considered to be instrumental in maintaining such a marginal instability (Jog and Solomon 1984; Bertin and Romeo 1988; Bertin *et al.* 1989). Jog and Solomon (1984) showed that the wavelength of the most unstable disk mode depends on the gas fraction. They found that the wavelengths of the most unstable disk modes at the solar Galactocentric distance should lie in the $1 - 5$ kpc interval, where 1 and 5 kpc correspond to a purely gaseous and purely stellar disk, respectively. Our result $\lambda = 2$ kpc suggests that both components play important part in the dynamics of our Galaxy.

ACKNOWLEDGMENTS

We are grateful to Yu.N.Efremov, A.V.Zasov, and A.V.Khoperskov for the discussions, as well as for the useful remarks and advice.

REFERENCES

Ambartsumian, V.A. *Astron. Zh.*, 1949, v. 26, p. 3 (rus).
Barbier-Brossat, M., Figon, P. *Astron. Astrophys. Suppl. Ser.*, 2000, v. 142, p. 217.
Berdnikov, L.N. *Perem. Zvezdy*, 1987, v. 22, p. 549.
Berdnikov, L.N., Chernin, A.D. *Astron. Lett.*, 1999, v. 25, p. 591
Berdnikov, L.N., Efremov, Yu.N. *Astron. Tsirk.*, 1985, No. 1388, p.1.
Berdnikov, L.N., Dambis, A.K., Vozyakova, O.V. *Astron. Astrophys. Suppl. Ser.*, 2000, v. 143, p. 211.
Bertin, G., Romeo, A.B. *Astron. and Astrophys.*, 1988, v. 195, p. 105.
Bertin, G., Lin, C.C., Lowe, S.A., Thurstans, R.P. *Astrophys. J.*, 1989, v. 338, p. 78.
Blaha, C., Humphreys, R.M. *Astron. J.*, 1989, v. 98, p. 1598.
Burton, W.B. *Astron. and Astrophys.*, 1971, v. 10, p. 76.
Burton, W.B., Bania, T.M. *Astron. and Astrophys.*, 1974, v. 33, p. 425.
Creze, M., Mennessier, M.O. *Astron. and Astrophys.*, 1973, v. 27, p. 281.
Dambis, A.K., Mel'nik, A.M., Rastorguev, A.S. *Astron. Lett.*, 1995, v. 21, p. 291.
Dambis, A.K., Mel'nik, A.M., Rastorguev, A.S. *Astron. Lett.*, 2001, v. 27, p. 58.
de Zeeuw, P. T., Hoogerwerf, R., de Bruijne, J. H. J., Brown, A. G. A., Blaauw, A. *Astron. J.*, 1999, v. 117, p. 354.
Efremov, Yu.N. *Astron. Astrophys. Trans.*, 1998, v. 15, p. 3.
Efremov, Yu.N., *Ochagi zvezdoobrazovaniya v galaktikakh* (Sites of Star Formation in Galaxies), Moscow: Nauka, 1989 (rus).
Efremov, Yu.N., Sitnik, T.G. *Sv. Astron. Lett.*, 1988, v. 14, p.347.
Elmegreen, B.G., *Astrophys. J.*, 1979, v. 231, p. 372.
Elmegreen, B.G., Wang, M., *Molecular Clouds in the Milky Way and External Galaxies. Lecture Notes in Physics, v. 315*, Eds. Dickman R.L., Snell R.L., Young J.S. Amherst, Massachusetts: Springer-Verlag, 1987, p. 240.
Fenkart, R.P., Binggeli, B. *Astron. Astrophys. Suppl. Ser.*, 1979, v. 35, p. 271.
Garmany, C.D., Stencel, R.E. *Astron. Astrophys. Suppl. Ser.*, 1992, v. 94, p. 211.
Gerasimenko, T.P. *Astron. Reports*, 1993, v. 37, p. 480.
Glushkova, E.V., Dambis, A.K., Mel'nik, A.M., Rastorguev, A.S. *Astron. Astrophys.*, 1998, v. 329, p. 514.
Humphreys, R.M., *The Large Scale Characteristics of the Galaxy, IAU Symp. no. 84* Ed. Burton W.B. Dordrecht: Reidel Publ. Company, 1979, p.93.
Jog, C.J., Solomon, P.M. *Astrophys. J.*, 1984, v. 276, p.114.

Kulikovskiĭ, P.G., Zvezdnaya astromomiya, Moscow: Nauka, 1985 (rus).
Lin, C.C.,Yuan, C., Shu, F.H. *Astrophys. J.*, 1969, v. 155, p. 721.
Mel'nik, A.M., Dambis, A.K., Rastorguev, A.S. *Astron. Lett.*, 1999, v. 25, p. 518.
Mel'nik, A.M., Efremov, Yu.N. *Astron. Lett.*, 1995, v. 21, p. 10.
Mel'nik, A.M., Sitnik T.G., Dambis, A.K., Efremov, Yu.N., Rastorguev, A.S. *Astron. Lett.*, 1998, v. 24, p. 594.
Mishurov, Yu.N., Pavlovskaya, E.D., Suchkov, A.A. *Sv. Astronony*, 1979, v.23, p.147.
Mishurov, Yu.N., Zenina, I.A., *Astron. Astrophys.*, 1999a, v. 341, p. 81.
Mishurov, Yu.N., Zenina, I.A., *Astron. Reports*, 1999b, v. 43, p. 487.
Mishurov, Yu.N., Zenina, I.A., Dambis, A.K., Mel'nik, A.M., Rastorguev, A.S. *Astron. Astrophys.*, 1997, v. 323, p. 775.
Morgan, W.W., Sharpless, S., Osterbrock, D. *Astron. J.*, 1952, v. 57, p. 3.
Press, W.H., Flannery, B.P., Teukoisky, S.A., Vetterling, W.T.) *Numerical Recipes: The art of scientific computing.* Cambridge: Cambridge Univ. Press, 1987.
Rastorguev, A.S., Durlevich, O.V., Pavlovskaya, E.D., Filippova, A.A., *Astron. Lett.*, 1994, v. 20, p. 591.
Roberts, W.W., *Astrophys. J.*, 1969, v. 158, p. 123.
Sitnik, T.G., Mel'nik, A.M., *Astron. Lett.*, 1996, v. v. 22, p. 422.
Sitnik, T.G., Mel'nik, A.M., *Astron. Lett.*, 1999, v. 25, p. 156.
Sitnik, T.G., Mel'nik, A.M., Pravdikova, V.V. *Astron. Reports*, 2001, v. 45, p. 34.
The Hipparcos and Tycho Catalogues. European Space Agency, 1997, v. 1–20.

Table 2. Residual velocities of OB associations

Association	l	b	r kpc	R kpc	V_R km s^{-1}	V_θ km s^{-1}	V_z, km s^{-1}	n_r	n_l	N
Sgr OB5	0.°0	-1.°2	2.4	4.7	7.5	9.0	8.0	2	3	31
Sgr OB1	7.6	-0.8	1.3	5.8	7.3	-5.4	1.0	37	29	66
Sgr OB7	10.7	-1.6	1.4	5.7	9.2	3.9	-14.4	3	2	4
Sgr OB4	12.1	-1.0	1.9	5.2	4.8	-0.0	-0.1	9	3	15
Ser OB1	16.7	0.1	1.5	5.7	13.0	-0.9	1.4	17	12	43
Sct OB3	17.3	-0.7	1.3	5.8	2.7	1.7	3.0	8	3	10
Ser OB2	18.2	1.6	1.6	5.6	13.7	-1.9	-3.7	7	5	18
Sct OB2	23.2	-0.5	1.6	5.7	26.3	-2.3	4.9	6	6	13
Vul OB1	60.4	0.0	1.6	6.5	6.4	-3.3	6.1	9	8	28
Vul OB4	60.6	-1.2	0.8	6.7	2.7	-0.1	-0.1	3	3	9
Cyg OB3	72.8	2.0	1.8	6.8	-14.5	-7.8	-4.0	30	18	42
Cyg OB1	75.8	1.1	1.5	6.9	-3.9	-8.3	1.2	34	14	71
Cyg OB9	77.8	1.8	1.0	7.0	-5.8	-12.2	0.2	10	8	32
Cyg OB8	77.9	3.4	1.8	7.0	-3.9	-13.9	12.8	9	10	21
Cyg OB4	82.7	-7.5	0.8	7.0	15.5	4.8	2.7	2	2	2
Cyg OB7	89.0	0.0	0.6	7.1	2.5	2.4	3.7	21	28	29
Lac OB1	96.7	-17.7	0.5	7.2	-3.6	-2.8	1.6	2	2	2
Cep OB2	102.1	4.6	0.7	7.3	-3.2	-0.1	2.8	37	47	59
Cep OB1	104.2	-1.0	2.8	8.2	-8.7	-14.3	3.1	17	24	58
Cas OB2	112.0	0.0	2.1	8.1	-19.0	-3.3	6.2	7	5	41
Cep OB3	110.4	2.6	0.7	7.4	-3.9	-4.9	0.5	18	15	26
Cas OB5	116.1	-0.5	2.0	8.2	-12.7	-2.7	-11.2	16	13	52
Cas OB4	120.1	-0.3	2.3	8.5	3.4	0.8	-6.4	7	7	27
Cas OB14	120.4	0.7	0.9	7.6	11.6	-2.7	2.3	4	3	8
Cas OB7	123.0	1.2	2.0	8.4	-10.3	-9.2	-2.7	4	8	39
Cas OB1	124.7	-1.7	2.0	8.4	-6.8	-2.5	-7.0	5	3	11
NGC 457	126.7	-4.4	2.0	8.4	-1.7	1.0	-6.7	4	2	4
Cas OB8	129.2	-1.1	2.3	8.7	2.3	2.5	-3.7	14	9	43
Per OB1	134.7	-3.2	1.8	8.5	-7.8	-12.2	-5.5	81	63	167
Cas OB6	135.0	0.8	1.8	8.4	-11.2	-6.8	-3.8	12	13	46
Cam OB1	141.1	0.9	0.8	7.7	-0.4	6.2	0.3	30	33	50
Cam OB3	147.0	2.8	2.6	9.4	9.5	-17.6	16.5	3	3	8
Per OB2	160.3	-16.5	0.3	7.4	16.0	9.6	-0.9	7	7	7
Aur OB1	173.9	0.1	1.1	8.2	-4.9	0.8	-2.7	26	20	36
Ori OB1	206.9	-17.7	0.4	7.4	8.2	0.5	0.3	62	59	70
Aur OB2	173.3	-0.2	2.4	9.5	-3.5	12.0	-2.8	4	2	20
Gem OB1	189.0	2.2	1.2	8.3	2.2	5.2	3.9	18	17	40
Mon OB1	202.1	1.1	0.6	7.6	6.3	0.5	1.8	7	7	7
Mon OB2	207.5	-1.6	1.2	8.2	-0.4	10.9	-0.5	26	18	32
CMa OB1	224.6	-1.6	1.1	7.9	7.2	3.5	-7.0	8	10	17
Coll 121	238.5	-8.4	0.6	7.4	5.9	-4.1	0.1	10	13	13
NGC 2362	237.9	-5.9	1.2	7.8	0.5	3.8	4.5	6	3	9
Coll 140	244.5	-7.3	0.3	7.2	-2.7	7.6	-1.5	5	6	6
Vela OB2	262.1	-8.5	0.4	7.2	2.2	-8.7	0.8	13	12	13
Vela OB1	264.9	-1.4	1.5	7.4	-0.5	-1.9	-2.5	18	18	46
Car OB1	286.5	-0.5	2.0	6.8	0.8	3.4	-2.2	39	18	126
Tr 16	287.3	-0.3	2.1	6.8	-2.3	-1.8	-2.6	5	2	18
Coll 228	287.6	-1.0	2.0	6.8	-6.6	10.0	-2.7	9	2	15
Car OB2	290.4	0.1	1.8	6.7	-4.3	2.2	0.3	22	12	59
Cru OB1	294.9	-1.1	2.0	6.5	-13.5	-6.1	-0.2	33	19	76
NGC 3766	294.1	-0.0	1.5	6.6	-7.3	7.9	0.5	2	2	12
Cen OB1	304.2	1.4	1.9	6.2	-16.8	0.6	-2.4	32	32	103
Hogg 16	307.5	1.4	1.5	6.3	-7.4	19.9	-11.7	3	3	5
NGC 5606	314.9	1.0	1.5	6.1	3.2	12.4	-6.6	3	2	5
Ara OB1A	337.7	-0.9	1.1	6.1	15.4	10.0	-3.8	8	10	53
Sco OB1	343.7	1.4	1.5	5.6	6.0	4.2	1.1	28	16	76
Sco OB2	351.3	19.0	0.1	7.0	-3.3	-3.1	0.7	10	10	10
HD 156154	351.3	1.4	2.1	5.0	-15.6	-5.1	-2.1	3	2	4
Sco OB4	352.7	3.2	1.0	6.2	-15.0	2.7	-3.2	7	4	11

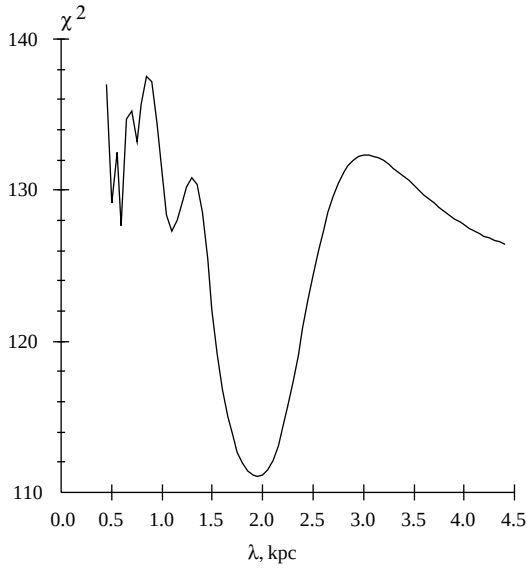

Figure 1: The function $\chi^2(\lambda)$ for the joint solution of the system of equations (3) and (4) for the entire sample of OB associations

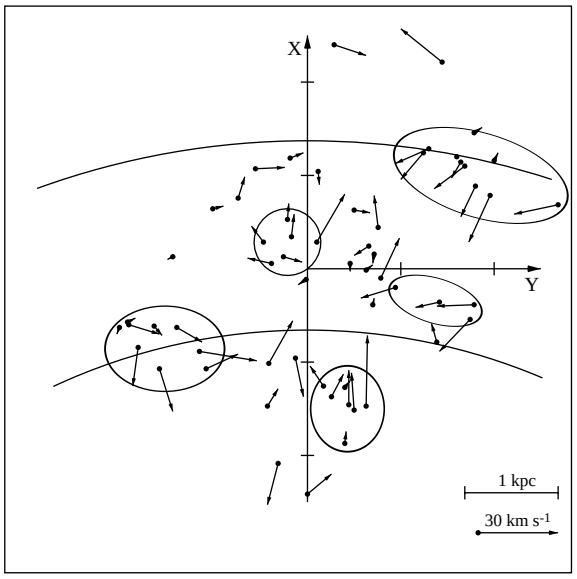

Figure 2: The field of space velocities of OB-associations projected onto the galactic plane. The X-axis is directed away from the Galactic center, and the Y-axis is in the direction of galactic rotation. The Sun is at the origin. The circular arcs correspond to the maximum radial component V_R of residual velocity toward the galactic center. One can see five star-forming regions where almost all OB-associations have the same direction of radial velocity V_R.

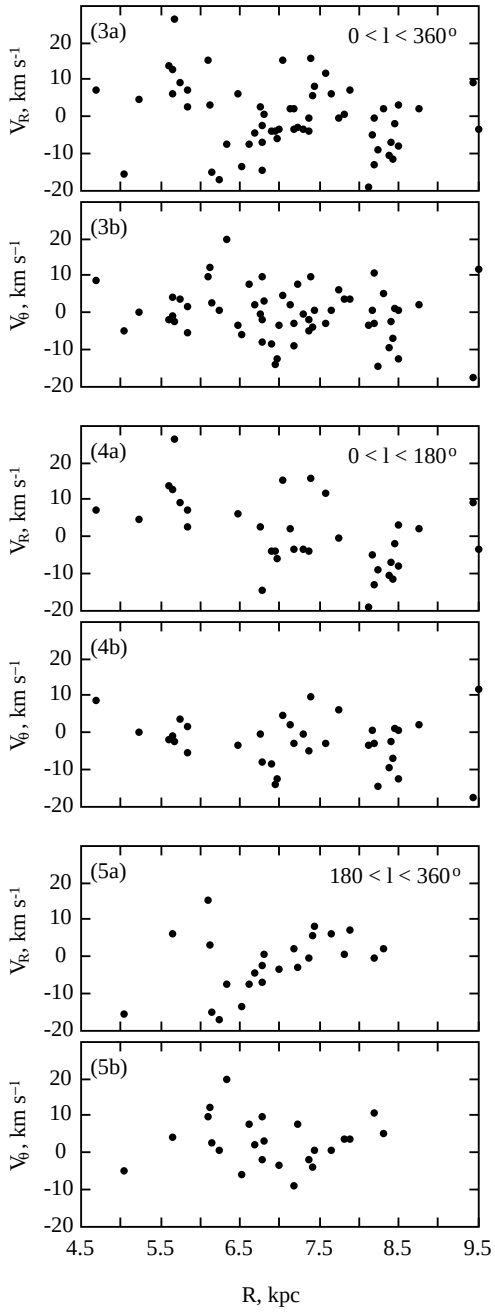

Figure 3: 4, 5. Residual velocities V_R and V_θ of OB-associations as a function of Galactocentric distance R. The whole sample and the regions $0 < l < 180°$ and $180 < l < 360°$ are concidered.

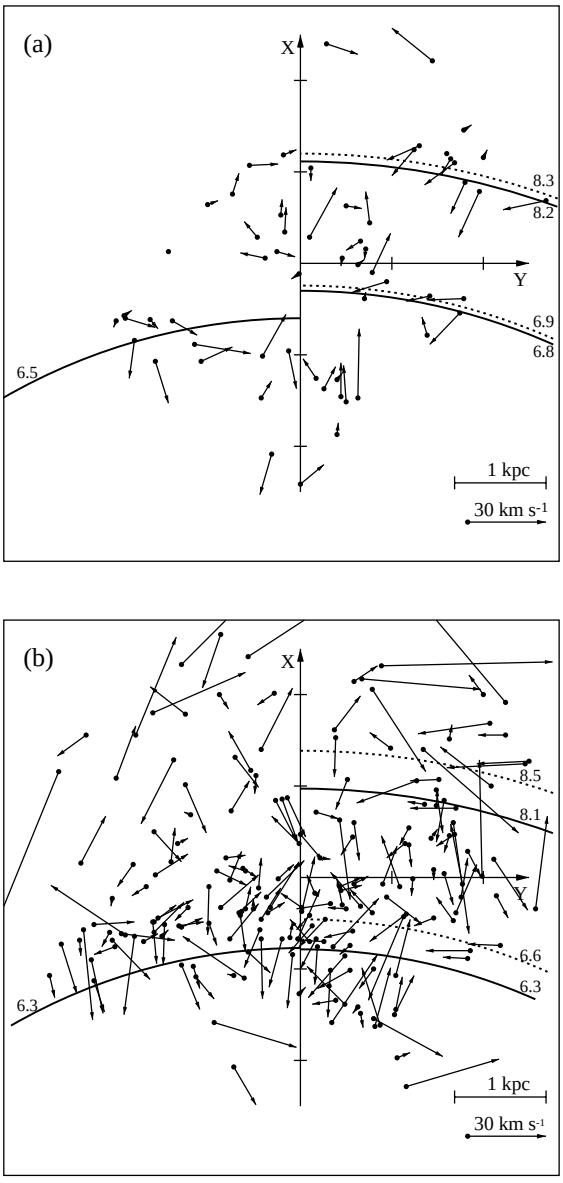

Figure 6: The field of residual velocities of (a) OB-associations and (b) Cepheids. The circular arcs correspond to the positions of the arm fragments as inferred from analyses of radial (solid line) and azimuthal (dashed line) residual velocities in the regions $30 < l < 180^\circ$ and $180 < l < 360^\circ$.